DOI: 10.1002/ ((please add manuscript number))
Article type: Communication

Flexible nanowire cluster as wearable colorimetric humidity sensor

Zhiqiang Wei, Zhang-Kai Zhou, Qiuyu Li, Jiancai Xue, Andrea Di Falco, Zhongjian Yang, Jianhua Zhou*, and Xuehua Wang*

Mr. Z. Wei, Prof. Z. K. Zhou, Mr. Q. Li, Mr. J. Xue, Prof. J. Zhou, Prof. X. Wang
State Key Laboratory of Optoelectronic Materials and Technologies, School of Physics, and Key Laboratroy of Sensing Technology and Biomedical Instruments of Guangdong Province, School of Enineering, Sun Yat-sen University, Guangzhou 510275, People's Republic of China
E-mail: zhouzhk@mail.sysu.edu.cn (Z. K. Zhou); zhoujh33@mail.sysu.edu.cn (J. Zhou)
Prof. Andrea Di Falco
SUPA, School of Physics and Astronomy, University of St. Andrews, North Haugh, St. Andrews, Fife, KY16 9SS, UK
Dr. Z. Yang
Hunan Key Laboratory of Super Microstructure and Ultrafast Process, School of Physics and Electronics, Central South University, Changsha, Hunan 410083, People's Republic of China

Keywords: functional wearable device; flexible sensor; film of nanowire cluster; colorimetric plasmonic device

Wearable plasmonic devices combine the advantages of high flexibility, ultrathinness, light weight, and excellent integration, with the optical benefits mediated by plasmon enhanced electric fields. However, two obstacles severely hinder further developments and applications of wearable plasmonic device. One is the lack of efficient approach to obtaining devices with robust anti-motion-interference property, *i. e.* the devices can work independently on the morphology changes of their working structures caused by arbitrary wearing conditions. The other issue is to seek a facile and high-throughput fabrication method to satisfy the financial requirement of industrialization. In order to overcome these two challenges, we develop a functional flexible film of nanowire cluster, which can be easily fabricated by taking the advantages of both conventional electrochemical and sputtering methods. Such flexible plasmonic films can be made into wearable devices working independently on shape changes induced by various wearing conditions (such as bending, twisting, and stretching).

Furthermore, due to plasmonic advantages of color-controlling and high-sensitivity to environment changes, the flexible film of nanowire cluster can be used to fabricate wearable items (such as bracelet, clothes, bag, or even commercial markers), with the ability of wireless visualization for humidity sensing.

1. Introduction

Wearable devices are attractive for opening up a comfortable, convenient, and secure life pattern, since they can be integrated with clothes,[1,2] eye glasses,[3] wristwatches,[4] and even skin sensors.[5,6] For example, previous reports on wearable devices have focused on sensing and signal processing for artificial electronic eye accessories,[7] artificial skin,[8-15] and health monitoring devices.[16-19] Generally, the rapid and flourishing progresses of wearable devices are mainly supported by the developments of various flexible devices, such as flexible batteries,[20] flexible sensors,[21,22] and stretchable display.[23] In addition, in order to pursue large signal-noise ratio, boosting working process, or realizing wirelessly active devices, plasmonic materials which are nanostructure that can sustain collective electron oscillations at their surface and therefore process an incomparable ability of controlling local electromagnetic field, have been widely applied into the fabrication of flexible devices. As consequences, notable achievements have been made due to the study of flexible plasmonic devices, such as tunable flexible plasmonic resonators,[24-26] flexible surface enhanced Raman scattering (SERS) devices,[27,28] plasmonic-enhanced polymer solar cells and organic photovoltaics,[29-31] enhanced multicolour photodetectors,[32] multifunctional flexible plasmonic nanorod array,[33] and plasmonic biosensor on various flexible substrates.[34-38] More importantly, with the advantages of light manipulation, plasmonic structure gives a colorful future for wireless visualized technique,[39,40] which has recently exhibited great advances in the field of wearable device fabrication.[41]

There are two main obstacles that hinder further development of flexible plasmonic

devices. On one hand, the traditional fabrication approaches for flexible plasmonic nanostructures typically involve standard nanolithography techniques, which exhibit shortcomings of high-cost and sophisticated manufacturing processes. On the other hand, since the plasmon properties are highly dependent on the geometrical morphology of plasmonic nanostructures, the functionalities of flexible plasmonic device may be greatly influenced when the devices are being bended, twisted, or stretched, which leads to microscopic structure changes of the working plasmonic structure.[24,28,37] This latter issue is so vital that it may curtail the deployment of any realistic application of plasmonic flexible devices for wearable equipments.

In order to address these two problems, we propose an easy and high-throughput strategy for fabricating flexible plasmonic sensors. We used a special kind of disordered anodic alumina oxide (DAAO) substrate and conventional sputtering technique to prepare nanowire cluster film (NWCF), and integrated the NWCF with polydimethylsiloxane (PDMS) to fabricate flexible devices. Our product can not only be scalable with good flexibility, but also can be made into wearable visualized sensing device which works independently on any bended or stretched conditions. Considering the inexpensive cost, the ease of fabrication, and the powerful functions, it is believed that our findings will be helpful for paving the way of flexible plasmonic device into the real industrial applications.

2. Results

The structure of nanowire cluster is fabricated by a one-step sputtering process on the DAAO substrate (**Figure 1**). As it is well-known that the sputtering technique is a convenient and widely used approach for depositing nanostructures on various substrates, and such approach is famous for its advantages of low equipment requirements, large sample area, and easy proceedings. However, due to the isotropic growth possibility of the sputtered metal ions, using normal flat substrates can only lead to the structure of nanofilm.[40] Although in our previous studies we were able to make nanoparticle film[42,43] by adjusting the sputtering

atmosphere, such strategies did not change the isotropic growth property of sputtering technique. Herein, by replacing the normal substrate with DAAO, we make the first successful trial to fabricate anisotropic nanostructure of nanowire by sputtering technique at room temperature. Our method expands the application of sputtering from isotropic to anisotropic[44], which will greatly extend the utilizations of sputtering technique in the field of nanofabrication and nanomaterials.

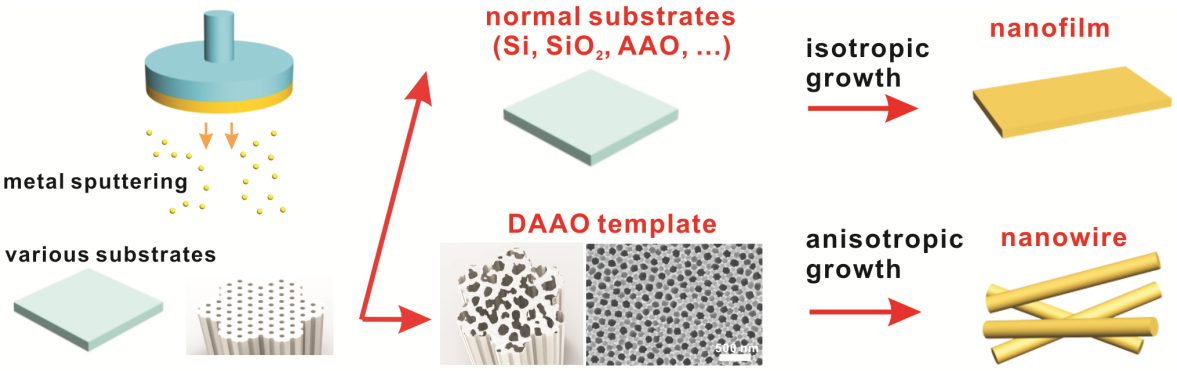

Figure 1. The difference between isotropic and anisotropic sputtering growth. Using normal substrates such as Si, SiO_2, and even normal AAO template, due to the isotropic growth possibility of the sputtered metal ions, only isotropic structure of nanofilm can be obtained. But, applying the DAAO as substrate, anisotropic structure of nanowire can be obtained by one-step sputtering process.

Figure 2 exhibits the sample images of Ag nanowire cluster and uncovers the possible growth mechanism. From the scanning electron microscopy (SEM) images of Figure 2a-c, one can see that with the increasing of deposition time, Ag nanowires gradually formed on the surface of DAAO substrate. It should be mentioned that since DAAO substrate can be easily dissolved by NaOH, such nanowires formed on the DAAO can also be released for further applications (Figure S1, transmission electron microscopy (TEM) images). In addition, after we changed the sputtering target material, it was also facile to fabricate nanowires of other materials, such as gold, platinum or aluminum (Figure S2, also shows the thicknesses of DAAO and Ag NWCF). After analyzing the above-mentioned SEM the TEM images, one can find the nanowires in the NWCF show small difference in diameter with an average value of

30 nm (Figure S3), despite of the lengths varying a lot (200-2000 nm). It is believed that the narrow walls and sharp tips on the surface of DAAO greatly benefit the growth of nanowire during the sputtering process (Figure 2d). At the beginning of the sputtering process, a thin layer of the deposited metal turns the DAAO substrate from perfectly insulating to conductive; additionally, since the sputtered substrate hosting the DAAO is charged with voltage, the sharp corners promote large local build-ups of the electric field, which makes the Ag ions preferentially deposit on the sharp tips. This assumption can be proved by the set of SEM images presented in Figure 2a. Here one can see that at the beginning of the nanowire cluster growth, short nanowires only assemble in correspondence of sharp protrusions (brighter and narrower parts of the DAAO, marked by red cycles). Subsequently, when the nanowires grow longer, they would fell down and lay on the surface of the DAAO (Figure 2b). Ag ions grow preferentially along the long direction of the nanowire because of the strong electric field around the ends of nanowire. Eventually, by increasing the deposition time, the structure of nanowire cluster forms on the surface of DAAO (Figure 2c).

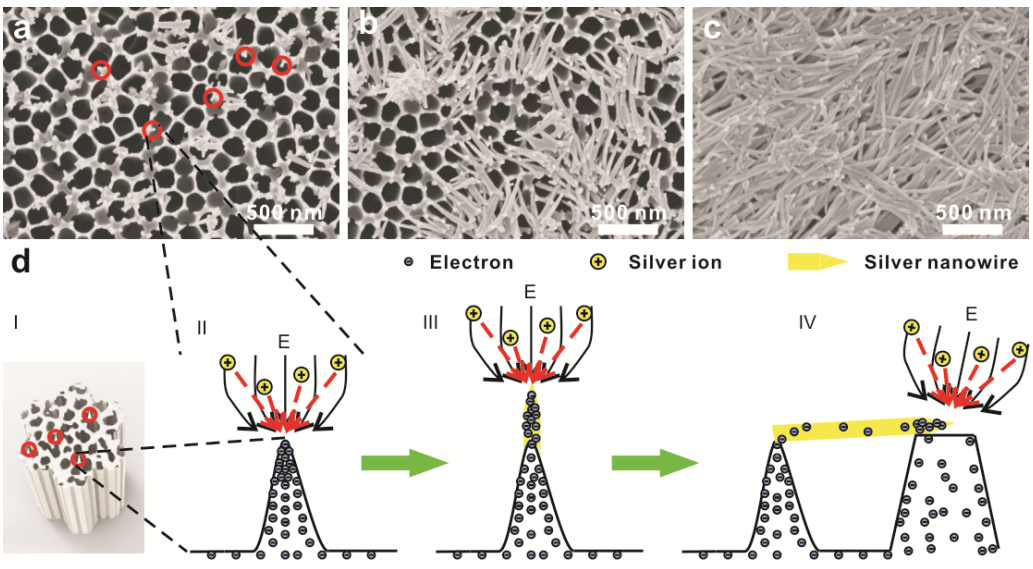

Figure 2. The nanowire cluster and its formation processes. (a)-(c) Deposited nanowires with the increasing of deposition time (a, at the beginning; b, after 30 s; c, after 100 s). (d) Scheme for the possible growth mechanism. The DAAO has numerous sharp tips on its surface (red cycles marked in part □ of figure d). In sputtering process, the sharp corners can arouse stronger electric fields than flat parts (part □ of figure d), which makes the Ag ions

preferentially deposit on the sharp tips (part □ of figure d). Therefore, at the beginning of nanowire cluster growth, short nanowires only assemble at the place with sharp protrusions (brighter and narrower parts of the DAAO, marked by red cycles in figure a). Subsequently, when the nanowires grow longer, they collapse down to the surface of DAAO (part □ of figure d). Since the ends of nanowires become new sharp tips, leading to large electric fields, Ag ions would grow along the length direction of the nanowire, making the nanowires get longer (figure b). At last, with the increase of deposition time, the structure of nanowire cluster forms on the surface of DAAO (figure c).

After the fabrication of NWCF, we transferred the composite of NWCF and DAAO substrate to the surface of a PDMS prepolymer mixture (Dow Corning, Sylgard 184, LOT: 0008315951), and following thermal treatment (the barrier layer of DAAO can prevent the PDMS penetrating into their nanoholes), a soft PDMS film with the structure of NWCF on its surface was obtained (**Figure 3**a). For simplicity, in our following text, we use flexible NWCF to describe the complex nanosystem of NWCF/DAAO/PDMS film. Due to the intrinsic advantages of both flexibility and durability of PDMS, the flexible NWCF can be bended or stretched arbitrarily without any damage to the working material of the NWCF (Figure 3b). In order to systematically investigate the flexibility of NWCF, we performed a series of experiments. Firstly, as Figure 3c presented, the extinction spectra show no differences in different curvature radii (ρ) (we also present a table to give the dependence relationship between ρ and the bending angle of θ, Table S1 in supporting information). Moreover, the extinction spectra of the flexible NWCF film also display similar shapes for different stretch rates (η, which is defined as the increased length divided by the original length) or after being bended for ever one thousand times (Figure 3d, original data are given in Figure S4). These experiments indicate that the NWCF exhibits outstanding stability and durability.

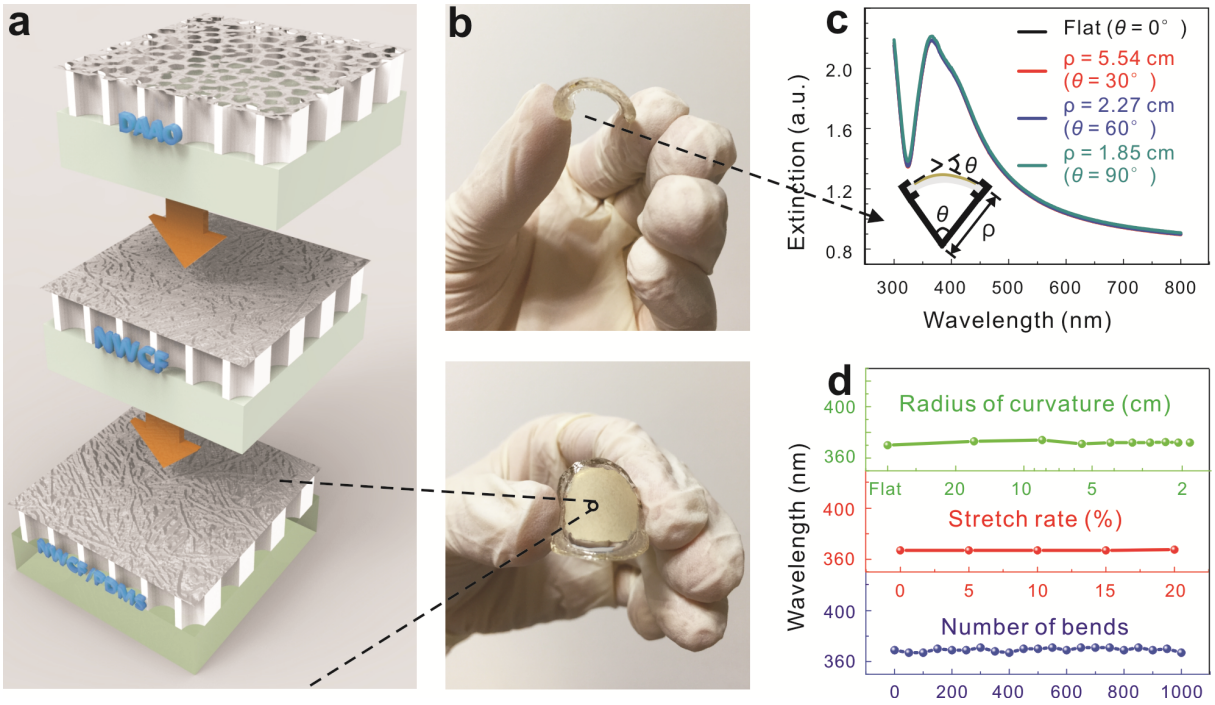

Figure 3. Preparation of the flexible NWCF and results of flexibility measurements. (a) Schematic of the preparation processes of the flexible NWCF. (b) Photo images of the as-obtained flexible NWCF with centimeter-size taken by a mobile phone (Meizu mx5). (c) Normalized extinction spectra of the flexible NWCF in different curvature radii (the definition of curvature radius is given by the inset of figure c). (d) The dependence of extinction peak wavelength on different testing conditions. Green line: the film has been bended to different curvature radii; red line: the film has been stretched for different stretch degrees; blue line: the film has been bended for different times.

Figure 3b,c demonstrate that the NWCF has robust anti-interference property, and in order to reveal the reason for such good characteristics, we carried out theoretical calculations. For an anisotropic nanostructure of nanowire, two plasmon modes can be sustained, which are the transverse and longitudinal plasmon modes (TPM and LPM), ascribed to the electron gas oscillating along the short and long axis of the nanowire, respectively (**Figure 4**). Therefore, the TPM and LPM depend on the effective lengths of the short and long axis, correspondingly. Generally, when the nanowires are embedded on some flexible device, they will be bended or stretched, and these conditions bring about obvious geometry changes, which may change the effective length on both transverse and longitudinal direction and therefore influence the

plasmon modes. However, after theoretical calculations by choosing the morphology structure parameters of typical experimental values, it is exciting to find that TPM and LPM exhibit completely different behaviors with geometry changes. Greatly different from the LPM, which is very sensitive to the length of the nanowire, the resonant peak of TPM is pinned at ~346 nm, despite of the length modification of the short axis from 20 to 40 nm (Figure 4a and b). In addition, when the silver nanowire is placed on the surface of an alumina template (Figure S5), one can find that the extinction spectra exhibit few changes with the increasing of length in long axis. Also, these simulation results are in good agreement with the experimental results, where only strong TPM can be found (Figure 3c). Furthermore, it is interesting to find that as one single nanowire structure extends to the structure of nanowire cluster, large electric field enhancements induced by plasmon coupling can be obtained at the sites between adjacent nanowires (Figure 4c). Because large electric field enhancements can always lead to high sensitive sensing and signal enhancements,[45,46] the NWCF with large working area can be a more suitable sensing material than a single nanowire.

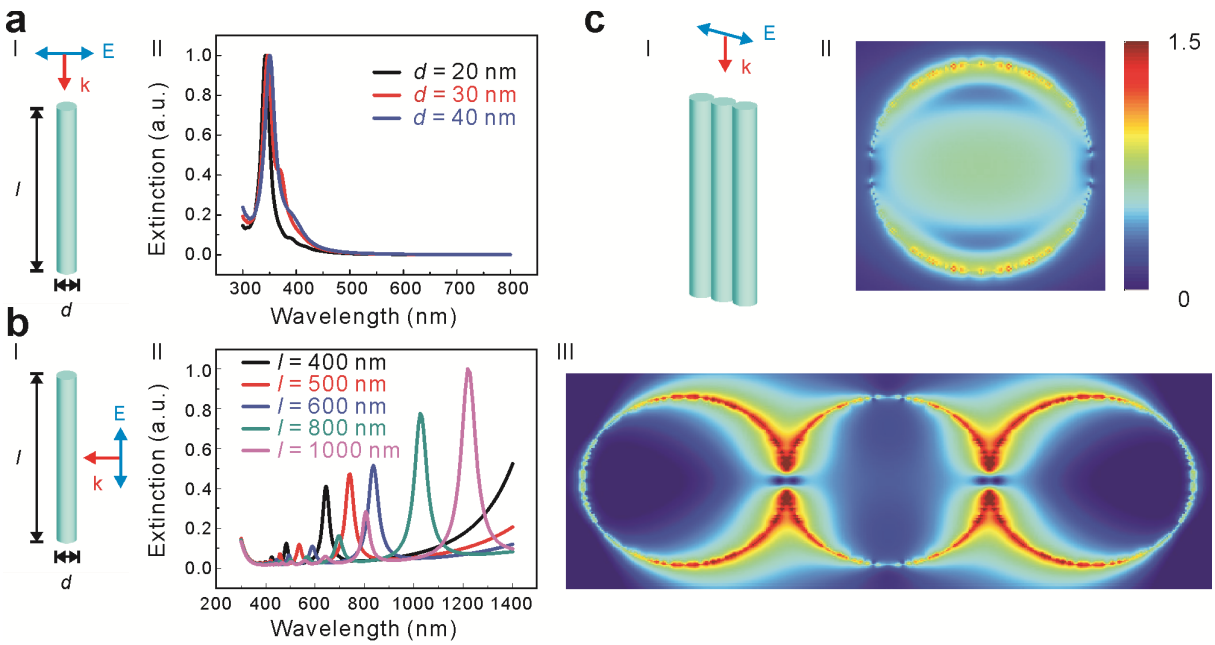

Figure 4. Calculated extinction spectra and electric field distributions of single Ag nanowire and a three-adjacent-nanowires cluster. (a) Numerical simulations of the TPM mode. (□) The schematics of simulation model and (□) the extinction spectra for a nanowire (l = 600 nm)

with different diameters. (b) Numerical simulations of the LPM mode. (□) The schematics of simulation model and (□) the extinction spectra for a nanowire (d =30 nm) with different lengths. (c) (□) is the schematics of simulation model; (□) and (□) are electric field distributions of a single nanowire and three adjacent nanowires at the extinction peak wavelengths of 346 nm and 416 nm, respectively. Each nanowire is set to be d =30 nm, l = 600 nm, and the electric field are given by logarithm form.

Based on the above experimental and theoretical findings, we can conclude that the photonic response of the flexible NWCF works independently on arbitrary bending or stretching conditions, which promotes them as an ideal material for plasmonic flexible sensing devices. This good characteristic roots from the fact that the related working plasmon resonant peak at ~370 nm is the TPM of Ag nanowire, and the extinction peak of this mode only depends on the diameter of a nanowire. The changes in the long axis or incident angle make few contributions to the TPM. In our samples, since the change in nanowire diameter is small, the TPM works independently on geometry changes caused by bending or stretching. Importantly, it should be pointed out that although many plasmonic flexible sensing devices have been proposed, the plasmonic properties of the majority of such devices may vary because of their morphology changes caused by stretching or bending. Therefore, the working data from these flexible sensing devices can only be obtained without morphological changes, *i. e.* maintaining the original length and bending curvature radius. Our approach removes such inconvenience, which makes us believe its great potentials in building real wearable plasmonic devices.

After the investigations of flexibility and plasmonic property, we applied the flexible NWCF into constructing a wearable sensing device. **Figure 5**a gives the normalized extinction spectra of the NWCF in different environments of refraction indexes, and the linear fitting of the extinction peak dependence on refraction index is in Figure 5b. Although the independence of TPM on shape changes is good for flexible sensor, the refractive index sensitivity (RIS) based on it is much lower than that mediated by LPM. So, seldom reports

about the TPM sensing devices are found. However, in this paper, due to the special nanostructure of nanowire cluster, the sensing ability of TPM is enhanced (as demonstrated in Figure S6), showing a RIS of 140.1 RIU/nm (Figure 5a and b). Such RIS value is comparable with the best result relied on LPM (Table S2 in Supporting Information). In addition, the experiments demonstrate that the RIS of NWCF is high enough to bring about obvious changes in extinction spectra when extremely small amount of water (0.028 mg/mm^2) is deposited on the NWCF, exhibiting two extinction peaks located at ~365 nm and ~400 nm, respectively (Figure 5c, the sample area is about ~500 mm^2, the weight of attached water can be measured by an analytical balance with precision of 0.1 mg). Many switching cycles have been performed, and the extinction spectra of NWCF show robust reproducibility, which means that the peak of extinction spectrum moves to ~400 nm when the NWCF is wet, and returns back to ~365 nm when the NWCF is dry (Figure 5d). Also, if we change the pure water to sweat or NaCl solution (using the equivalent concentration of NaCl in sweat), the same drifting cycles of peak wavelength can still be observed. Additionally, it is found that its response time is within ~1 s. These facts encourage us to make a sport bracelet with the flexible NWCF. In brief, we put a paper mask with a star shape hole onto the DAAO substrate before silver sputtering, and then we could obtain a NWCF with star pattern. After using the above-mentioned method of replacing Al substrate with a PDMS film (Figure 3a), the sport bracelet was fabricated. Referring to the working performance of this bracelet, the star pattern shows the color of bright white at the beginning, and the whole star changes to bright yellow after ~20 min of running, because of sweating (Figure 5e,f). In addition, after the NWCFs go through different hydrophobic treatments, the amount of water that can make the NWCF change color will be increased. By arranging several NWCFs with different hydrophobic treatments together, one is able to deduce amount of sweat which is related to sport conditions (Figure S7). Such wearable active plasmonic sensor not only possesses the advantages of wirelessly visualizing, but also can be easily fabricated with large scale. Furthermore, except

for the bracelet, the flexible NWCF can also be used in clothes design or commercial logo decorations. Also, it is found that small parts of silver oxide (Ag_2O) are generated on the NWCF surface (Figure S8) which is stable under ambient condition.[47,48] As a result, the Ag NWCF not only exhibits remarkable mechanical durability (e.g. bending and stretching), bus also shows good stability under ambient condition.

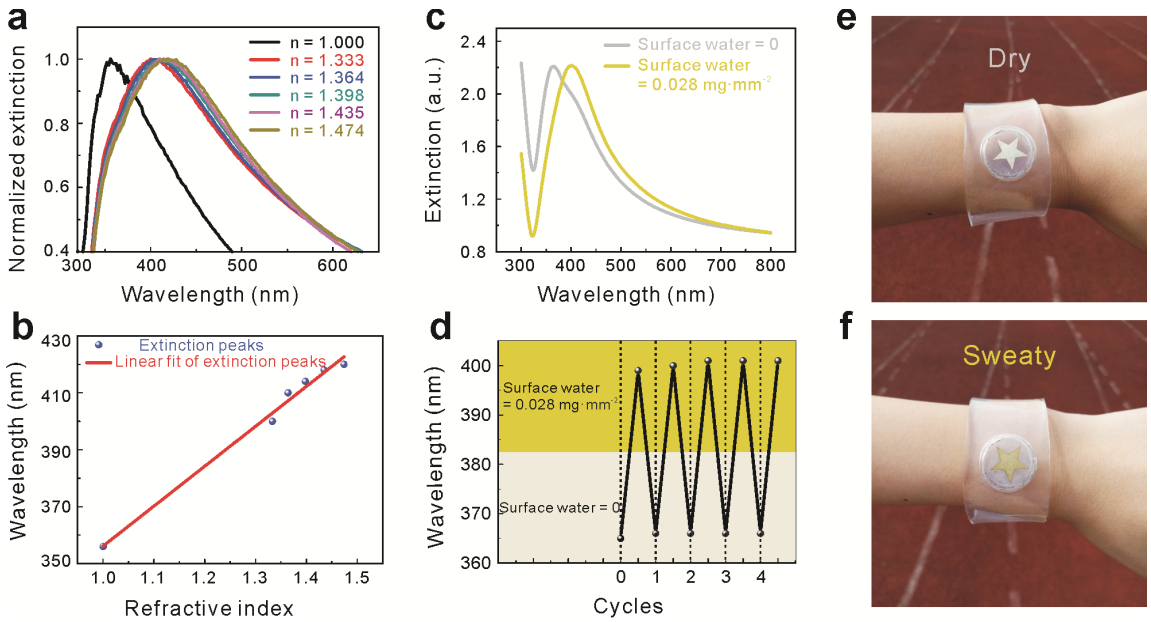

Figure 5. Wearable sensing bracelet based on the flexible NWCF. a) Normalized extinction spectra of the NWCF in environments of different reflective indexes. b) The linear fitting result of the relationship between the extinction peak wavelength and the environmental refractive index. c) Extinction spectra of the flexible NWCF under different environments of air humidity. d) Reversible shift of extinction peak wavelength of the flexible NWCF in repeated cycles of alternatively with and without water (0.028 mg/mm^2) on its surface. e) and f) Photo images of the as-obtained wearable sensing bracelet in dry and sweaty conditions.

3. Conclusion

In summary, we proposed a novel strategy to generate functional nanostructure of flexible nanowire cluster film, which was easily fabricated by the widely-used conventional sputtering technique with the help of a disordered alumina substrate. Such strategy successfully obtained metallic (*e.g.* Al, Ag, Au, Pt) anisotropic structures of nanowire by sputtering at room temperature, which is rare in previous reports. Because of the advantages of sputtering, this

new approach enables us to fabricate samples in centimeter-scale with simple procedures. Also, using the transverse plasmon mode of nanowire clusters for sensing, such flexible plasmonic films exhibited high sensitivity and robust anti-motion-interference merits when it was applied to build humidity sensors, showing a sensing threshold of 0.028 mg/cm^2 and working completely independently on arbitrary bending or stretching conditions. Furthermore, we made the flexible nanowire cluster film into a bracelet to monitor sport sweating conditions, and found that the sensing information of the wearable plasmonic bracelet can be wirelessly visualized. Based on those merits, it is believed that the functional structure of nanowire cluster film, together with its fabrication strategy, will find great applications in wearable sensors, flexible display devices and high surface-area catalyst.

4. Experimental Section

Preparation of the flexible Ag nanowire cluster film: The Ag nanowire cluster was fabricated on the DAAO substrates. The DAAO substrates were previously prepared using an optimized two-step anodization process. Prior to the anodization, the aluminum sheets (purity 99.999%) were degreased in acetone and electrically polished under a constant voltage of 16 V for 4 min in a mixture of $HClO_4$ and C_2H_5OH at 0 °C. In the first anodization step, the polished aluminum sheet was exposed to a $H_2C_2O_4$ solution (0.3 M) under a constant voltage of 40 V at 4 °C for 3 h. The alumina layer produced in the first anodization process was then removed by wet chemical etching in a mixture of phosphoric acid (0.15 M) and chromic acid (0.60 M) at 60 °C for 1 h, but the aluminum sheet was still reserved for a second anodization. In the second anodization step, the etched aluminum sheet was anodized using 10 wt% H_3PO_4. The growth voltage was set to 40 V and lasted for 3 min. Thereafter the voltage was quickly raised to 80 V and lasted for another 2.5 h. During these processes the preparation temperature was controlled around 20 °C. After the growth of the DAAO substrate, the Ag nanowire cluster was obtained by sputtering under a current of 60 mA (Q150 T ES, Quorum).

In particular, we put a paper with a star shape hole onto the DAAO substrate before silver sputtering to fabricate the sport bracelet in Fig. 5e and 5f. Lastly, in order to make flexible NWCF, the Al substrate on which the DAAO is grown was removed by $CuCl_2$ (1.5 M) and replaced with PDMS. After heating to 70 °C and retaining this temperature for 5 h, the flexible Ag nanowire cluster film was formed.

Optical and morphology characterization: All extinction spectra were measured on an ultraviolet/visible/near-infrared spectrometer (Lambda 950, PerkinElmer). In order to measure the extinction spectra under different conditions, a special box was made to fix the sample when it was being bended or stretched. The sample was round in shape with a diameter of ~3.5 cm. In the humidity sensing measurement, the water was attached on by exposing the sample to water steam. The SEM images were taken by a Zeiss Auriga-39-34 (Oberkchen, Germany) microscope operating at 5.0 kV.

Numerical simulations: The simulation results shown in Figure 4 were calculated with Finite-difference Time-domain (FDTD) method, using a commercially available FDTD simulation software package from Lumerical Solutions. The light source was total-field scattered-field, the mesh step was set as 0.2×0.2×0.2 nm and the boundary condition was perfectly matched layer (PML). The permittivity of silver was taken from Palik.[49]

Supporting Information

Supporting Information is available from the Wiley Online Library or from the author.

Acknowledgements

This work was supported by Ministry of Science and Technology of China (2016YFA0301300), National Natural Science Foundation of China (61675237, 11511130056, 21405183), the Guangdong Natural Science Foundation (2014A030313140, 2016A030312012), Guangzhou science and technology projects (201607020023), and the fundamental research funds for the central universities (16lgjc85, 16lgjc62). Zhiqiang Wei and Zhang-Kai Zhou contributed equally to this work.

Received: ((will be filled in by the editorial staff))
Revised: ((will be filled in by the editorial staff))
Published online: ((will be filled in by the editorial staff))

[1] Y. Meng, Y. Zhao, C. Hu, H. Cheng, Y. Hu, Z. Zhang, G. Shi, L. Qu, *Adv. Mater*. **2013**, *25*, 2326.

[2] J. Zhong, Y. Zhang, Q. Zhong, Q. Hu, B. Hu, Z. L. Wang, J. Zhou, *ACS Nano* **2014**, *8*, 6273.

[3] S. Feng, R. Caire, B. Cortazar, M. Turan, A. Wong, A. Ozcan, *ACS Nano* **2014**, *8*, 3069.

[4] D. J. Wile, R. Ranawaya, Z. H. Kiss, *J. Neurosci. Methods* **2014**, *230*, 1.

[5] D. H. Kim, N. Lu, R. Ma, Y. S. Kim, R. H. Kim, S. Wang, J. Wu, S. M. Won, H. Tao, A. Islam, K. J. Yu, T. I. Kim, R. Chowdhury, M. Ying, L. Xu, M. Li, H. J. Chung, H. Keum, M. McCormick, P. Liu, Y. W. Zhang, F. G. Omenetto, Y. Huang, T. Coleman, J.A. Rogers, *Science* **2011**, *333*, 838.

[6] X. Wang, Y. Gu, Z. Xiong, Z. Cui, T. Zhang, *Adv. Mater.* **2014**, *26*, 1336.

[7] Y. M. Song, Y. Xie, V. Malyarchuk, J. Xiao, I. Jung, K. J. Choi, Z. Liu, H. Park, C. Lu, R.-H. Kim, R. Li, K. B. Crozier, Y. Huang, J. A. Rogers, *Nature* **2013**, *497*, 95.

[8] K. Takei, T. Takahashi, J. C. Ho, H. Ko, A. G. Gillies, P. W. Leu, R. S. Fearing, A. Javey, *Nat. Mater.* **2010**, *9*, 821.

[9] C. Wang, D. Hwang, Z. Yu, K. Takei, J. Park, T. Chen, B. Ma, A. Javey, *Nat. Mater.* **2013**, *12*, 899.

[10] S. C. B. Mannsfeld, B. C.-K. Tee, R. M. Stoltenberg, C. V. H. H. Chen, S. Barman, B. V. O. Muir, A. N. Sokolov, C. Reese, Z. Bao, *Nat. Mater.* **2010**, *9*, 859.

[11] M. L. Hammock, A. Chortos, B. C. K. Tee, J. B. H. Tok, Z. Bao, *Adv. Mater.* **2013**, *25*, 5997.

[12] R. C. Webb, A. P. Bonifas, A. Behnaz, Y. Zhang, K. J. Yu, H. Cheng, M. Shi, Z. Bian, Z. Liu, Y. S. Kim, W. H. Yeo, J. S. Park, J. Song, Y. Li, Y. Huang, A. M. Gorbach, J. A. Rogers, *Nat. Mater*. **2013**, *12*, 938.

[13] M. Kaltenbrunner, T. Sekitani, J. Reeder, T. Yokota, K. Kuribara, T. Tokuhara, M. Drack, R. Schwodiauer, I. Graz, S. Bauer-Gogonea, S. Bauer, T. Someya, *Nature* **2013**, *499*, 458.

[14] T. Someya, T. Sekitani, S. Iba, Y. Kato, H. Kawaguchi, T. Sakurai, *Proc. Natl. Acad. Sci. USA* **2004**, *101*, 9966.

[15] W. Wu, X. Wen, Z. L. Wang, *Science* **2013**, *340*, 952.

[16] G. Schwartz, B. C. K. Tee, J. Mei, A. L. Appleton, D. H. Kim, H. Wang, Z. Bao, *Nat. Commun.* **2013**, *4*, 1859.

[17] C. Pang, G. Y. Lee, T. Kim, S. M. Kim, H. N. Kim, S. H. Ahn, K. Y. Suh, *Nat. Mater.* **2012**, *11*, 795.

[18] T. Yamada, Y. Hayamizu, Y. Yamamoto, Y. Yomogida, A. Izadi-Najafabadi, D. N. Futaba, K. Hata, *Nat. Nanotechnol.* **2011**, *6*, 296.

[19] D. H. Kim, N. Lu, R. Ghaffari, Y. S. Kim, S. P. Lee, L. Xu, J. Wu, R. H. Kim, J. Song, Z. Liu, J. Viventi, B. de Graff, B. Elolampi, M. Mansour, M. J. Slepian, S. Hwang, J. D. Moss, S. M. Won, Y. Huang, B. Litt, J. A. Rogers, *Nat. Mater.* **2011**, *10*, 316.

[20] G. Zhou, F. Li, H. Cheng, *Energy Environ. Sci*. **2014**, *7*, 1307.

[21] M. C. McAlpine, H. Ahmad, D. W. Wang, J. R. Heath, *Nat. Mater.* **2007**, *6*, 379.

[22] O. Vazquez-Mena, T. Sannomiya, M. Tosun, L. G. Villanueva, V. Savu, J. Voros, J. Brugger, *ACS Nano* **2012**, *6*, 5474.

[23] T. Sekitani, H. Nakajima, H. Maeda, T. Fukushima, T. Aida, K. Hata, T. Someya, *Nat. Mater*. **2009**, *8*, 494.

[24] H. G. Yan, X. S. Li, B. Chandra, G. Tulevski, Y. Q. Wu, M. Freitag, W. J. Zhu, P. Avouris, F. N. Xia, *Nat. Nanotechnol.* **2012**, *7*, 330.

[25] P. Reader-Harris, A. Di Falco, *ACS Photonic* **2014**, *1*, 985.

[26] M. Kahraman, P. Daggumati, O. Kurtulus, E. Seker, S. Wachsmann-Hogiu, *Sci. Rep.* **2013**, *3*, 3396.

[27] J. Leem, M. C. Wang, P. Kang, S. Nam. *Nano Lett*. **2015**, *15*, 7684.

[28] H. Kang, C. J. Heo, H. C. Jeon, S. Y. Lee, S. M. Yang, *ACS Appl. Mater. Inter.* **2013**, *5*, 4569.

[29] K. Yao, X. K. Xin, C. C. Chueh, K. S. Chen, Y. X. Xu, A. K. Y. Jen, *Adv. Funct. Mater.* **2015**, *25*, 567.

[30] L. Britnell, R. M. Ribeiro, A. Eckmann, R. Jalil, B. D. Belle, A. Mishchenko, Y. J. Kim, R. V. Gorbachev, T. Georgiou, S. V. Morozov, A. N. Grigorenko, A. K. Geim, C. Casiraghi, A. H. Castro Neto, K. S. Novoselov, *Science* **2013**, *340*, 1311.

[31] Q. Gan, F. J. Bartoli, Z. H. Kafafi, *Adv. Mater.* **2013**, *25*, 2385.

[32] Y. Liu, R. Cheng, L. Liao, H. L. Zhou, J. Bai, G. Liu, L. Liu, Y. Huang, X. Duan, *Nat. Commun.* **2011**, *2*, 579.

[33] J. Li, Z. Wei, J. Xu, Z. K. Zhou, D. Kong, J. Liu, J. Liu, X. Duan, J. Xue, J. Wang, X. Wang, *Adv. Opt. Mater*. **2015**, *3*, 1355.

[34] L. Li, H. T. Lin, S. T. Qiao, Y. Zou, S. Danto, K. Richardson, J. D. Musgraves, N. S. Lu, J. J. Hu, *Nat. Photonics* **2014**, *8*, 643.

[35] J. H. Du, S. F. Pei, L. P. Ma, H. M. Cheng, *Adv. Mater.* **2014**, *26*, 1958.

[36] A. N. Grigorenko, M. Polini, K. S. Novoselov, *Nat. Photonics* **2012**, *6*, 749.

[37] S. Aksu, M. Huang, A. Artar, A. A. Yanik, S. Selvarasah, M. R. Dokmeci, H. Altug, *Adv. Mater.* **2011**, *23*, 4422.

[38] X. P. Shen, T. J. Cui, D. Martin-Cano, F. J. Garcia-Vidal, *Proc. Natl. Acad. Sci. USA.* **2013**, *110*, 40.

[39] K. Kumar, H. Duan, R. S. Hegde, S. C. W. Koh, J. N. Wei, J. K. W. Yang, *Nat. Nanotech.* **2012**, *7*, 557.

[40] J. Xue, Z. K. Zhou, Z. Wei, R. Su, J. Lai, J. Li, C. Li, T. Zhang, X H. Wang, *Nat. Commun.* **2015**, *6*, 8906.

[41] X. Zhu, C. Vannahme, E. Højlund-Nielsen, N. A. Mortensen, A. Kristensen, *Nat. Nanotech.* **2016**, *11*, 325.

[42] Z. K. Zhou, X. N. Peng, Z. J. Yang, Z. S. Zhang, M. Li, X. R. Su, Q. Zhang, X. Y. Shan, Q. Q. Wang, Z. Y. Zhang, *Nano Lett.* **2011**, *11*, 49.

[43] H. Xu, J. Liu, X. Duan, J. Li, J. Xue, X. Sun, Y. Cai, Z. K. Zhou, X. Wang, *Opt. Mater. Express.* **2014**, *4*, 2586.

[44] J. Zhou, J. Zeng, J. Grant, H. Wu, Y. Xia, *Small* **2011**, *7*, 3308.

[45] I. Abdulhalim, *Small* **2014**, *10*, 3499.

[46] J. S. Miao, W. D. Hu, Y. L. Jing, W. J. Luo, L. Liao, A. L. Pan, S. W. Wu, J. X. Cheng, X. S. Chen, W. Lu, *Small* **2015**, *11*, 2392.

[47] G. I. N. Waterhouse, G. A. Bowmaker, J. B. Metson, *Appl. Surf. Sci.* **2001**, 183, 191.

[48] J. Zuo, J. Rao, G. Eggeler, *Mater. Chem. Phys.* **2014**, 145, 90.

[49] E. D. Palik, G. Ghosh, *Handbook of Optical Constants of Solids*, Academic, Manhattan, NY, USA **1998**.

Figures

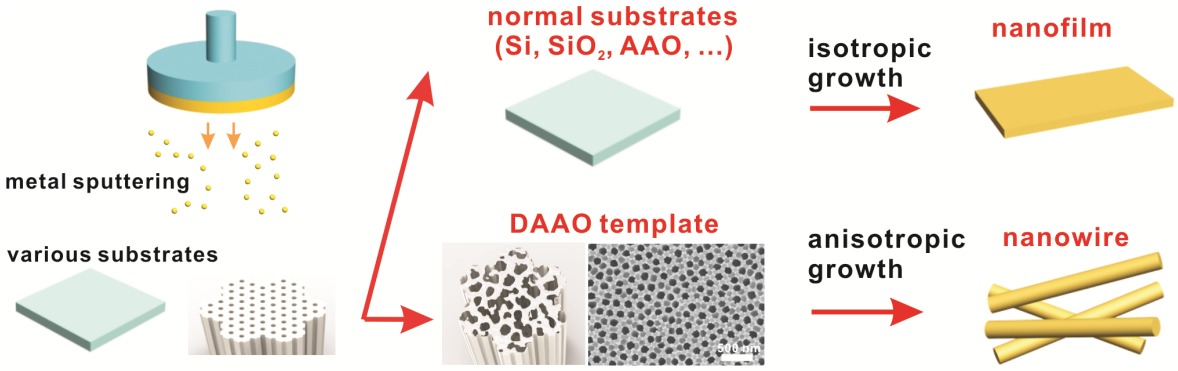

Figure 1. The difference between isotropic and anisotropic sputtering growth. Using normal substrates such as Si, SiO_2, and even normal AAO template, due to the isotropic growth possibility of the sputtered metal ions, only isotropic structure of nanofilm can be obtained. But, applying the DAAO as substrate, anisotropic structure of nanowire can be obtained by one-step sputtering process.

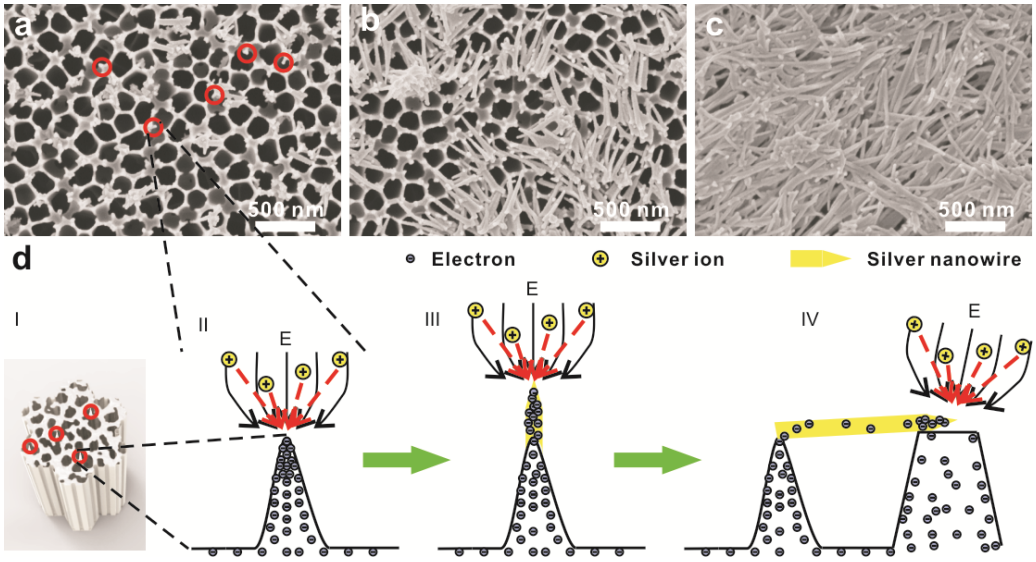

Figure 2. The nanowire cluster and its formation processes. (a)-(c) Deposited nanowires with the increasing of deposition time (a, at the beginning; b, after 30 s; c, after 100 s). (d) Scheme for the possible growth mechanism. The DAAO has numerous sharp tips on its surface (red cycles marked in part □ of figure d). In sputtering process, the sharp corners can arouse stronger electric fields than flat parts (part □ of figure d), which makes the Ag ions preferentially deposit on the sharp tips (part □ of figure d). Therefore, at the beginning of nanowire cluster growth, short nanowires only assemble at the place with sharp protrusions (brighter and narrower parts of the DAAO, marked by red cycles in figure a). Subsequently, when the nanowires grow longer, they collapse down to the surface of DAAO (part □ of figure d). Since the ends of nanowires become new sharp tips, leading to large electric fields, Ag ions would grow along the length direction of the nanowire, making the nanowires get longer (figure b). At last, with the increase of deposition time, the structure of nanowire cluster forms on the surface of DAAO (figure c).

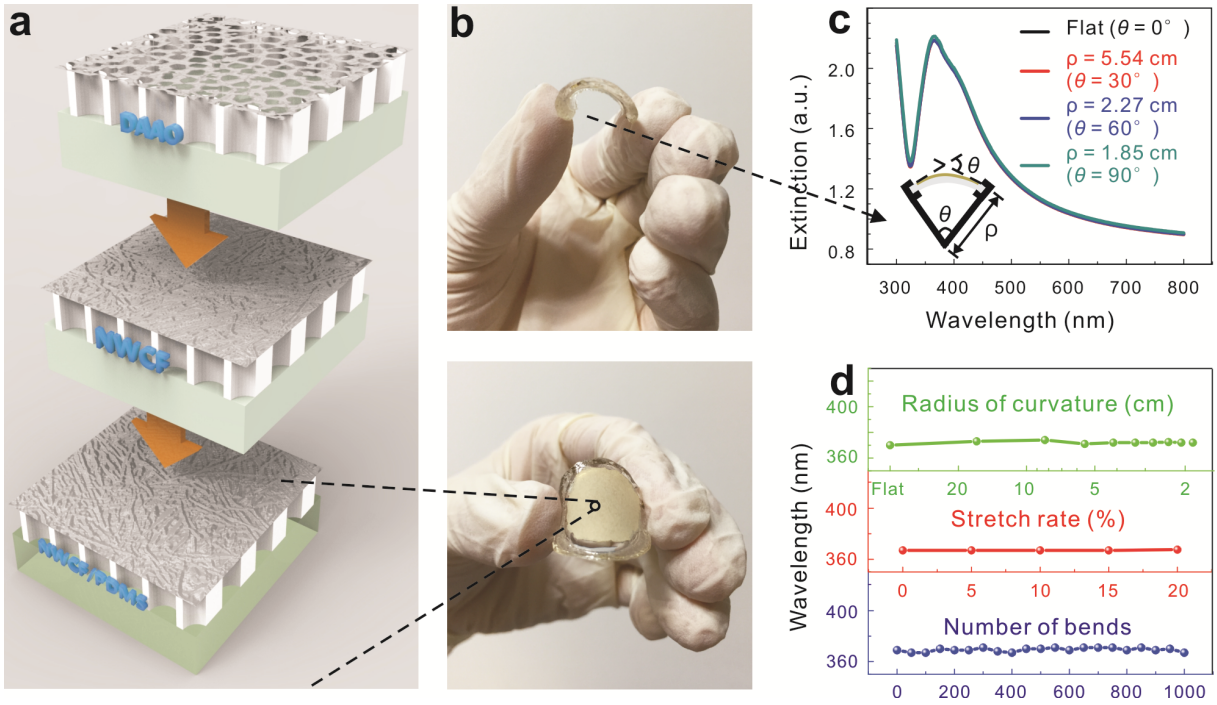

Figure 3. Preparation of the flexible NWCF and results of flexibility measurements. (a) Schematic of the preparation processes of the flexible NWCF. (b) Photo images of the as-obtained flexible NWCF with centimeter-size taken by a mobile phone (Meizu mx5). (c) Normalized extinction spectra of the flexible NWCF in different curvature radii (the definition of curvature radius is given by the inset of figure c). (d) The dependence of extinction peak wavelength on different testing conditions. Green line: the film has been bended to different curvature radii; red line: the film has been stretched for different stretch degrees; blue line: the film has been bended for different times.

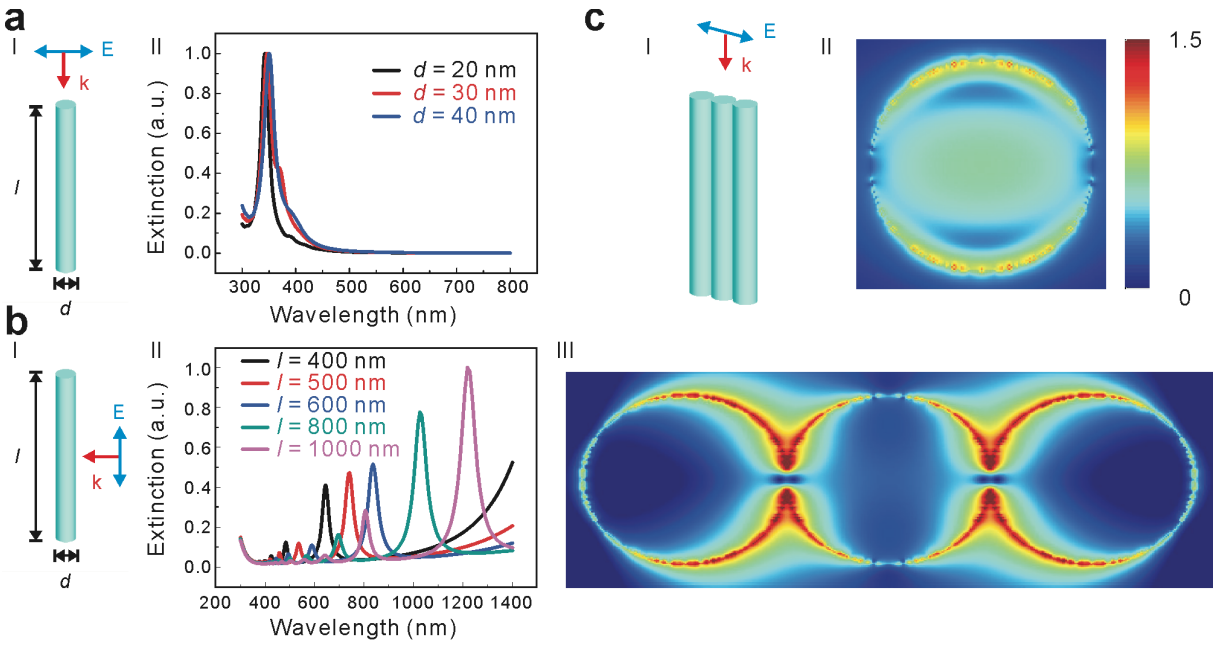

Figure 4. Calculated extinction spectra and electric field distributions of single Ag nanowire and a three-adjacent-nanowires cluster. (a) Numerical simulations of the TPM mode. (□) The schematics of simulation model and (□) the extinction spectra for a nanowire (l = 600 nm) with different diameters. (b) Numerical simulations of the LPM mode. (□) The schematics of simulation model and (□) the extinction spectra for a nanowire (d =30 nm) with different lengths. (c) (□) is the schematics of simulation model; (□) and (□) are electric field distributions of a single nanowire and three adjacent nanowires at the extinction peak wavelengths of 346 nm and 416 nm, respectively. Each nanowire is set to be d =30 nm, l = 600 nm, and the electric field are given by logarithm form.

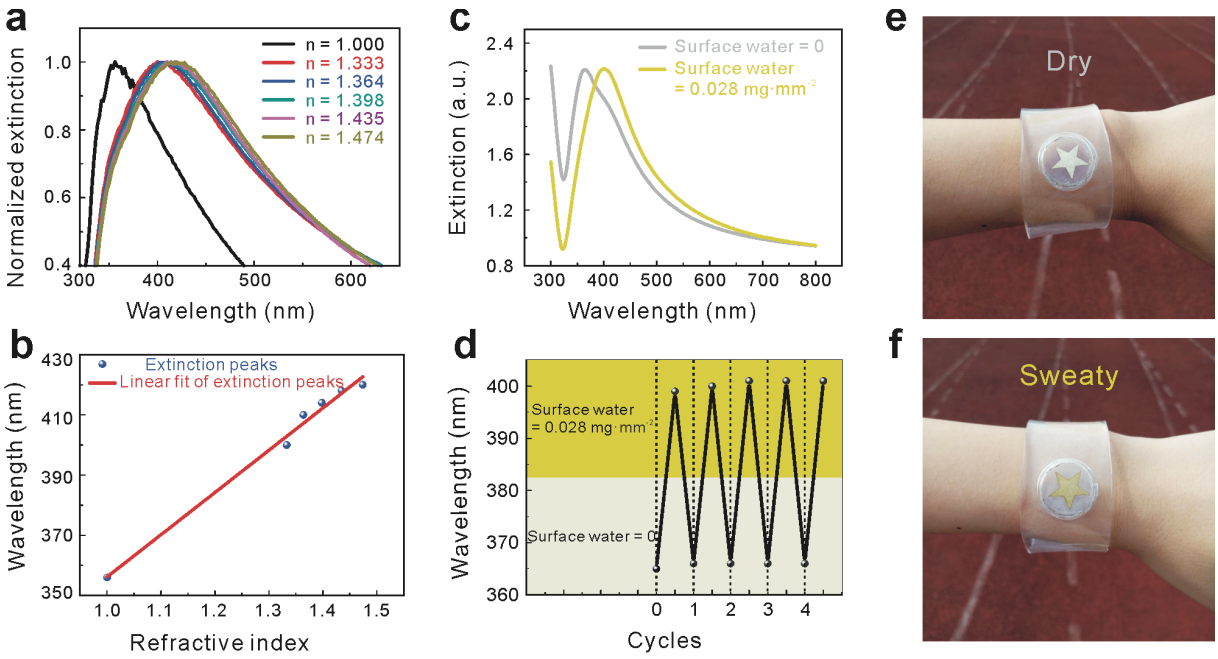

Figure 5. Wearable sensing bracelet based on the flexible NWCF. a) Normalized extinction spectra of the NWCF in environments of different reflective indexes. b) The linear fitting result of the relationship between the extinction peak wavelength and the environmental refractive index. c) Extinction spectra of the flexible NWCF under different environments of air humidity. d) Reversible shift of extinction peak wavelength of the flexible NWCF in repeated cycles of alternatively with and without water (0.028 mg/mm^2) on its surface. e) and f) Photo images of the as-obtained wearable sensing bracelet in dry and sweaty conditions.